

Pure Spin Current Injection in Hydrogenated Graphene Structures

Reinaldo Zapata-Peña,¹ Bernardo S. Mendoza,¹ and Anatoli I. Shkrebtii²

¹*Centro de Investigaciones en Óptica, León, Guanajuato 37150, México*

²*University of Ontario, Institute of Technology, Oshawa, ON, L1H 7L7, Canada*

(Dated: August 18, 2017)

Abstract

We present a theoretical study of spin-velocity injection (SVI) of a pure spin current (PSC) induced by a linearly polarized light that impinges normally on the surface of two 50% hydrogenated noncentrosymmetric two-dimensional 2D graphene structures. The first structure, hydrogenated at only one side, labeled Up, also known as graphone, and the second, one labelled Alt, is 25% hydrogenated at both sides. The hydrogenation opens an energy gap in both structures. We analyze two possibilities: the first one is by fixing the spin along a chosen direction, and the resulting SVI is calculated. Secondly, we choose the SVI direction along the surface plane, and calculate the resulting spin orientation. This is done by changing the energy $\hbar\omega$ and polarization angle α of the incoming light. The results are calculated within a full electronic band structure scheme using the Density Functional Theory (DFT) in the Local Density Approximation (LDA). The maxima of the spin-velocities are reached when $\hbar\omega = 0.084$ eV and $\alpha = 35^\circ$ for the Up structure, and $\hbar\omega = 0.720$ eV and $\alpha = 150^\circ$ for the Alt geometry. We find a speed of 668 Km/s and 645 Km/s for the Up and the Alt structures, respectively, when the spin points perpendicularly to the surface. Also, the response is maximized by fixing the spin-velocity direction along a high symmetry axis, obtaining a speed of 688Km/s with the spin pointing at 13° from the surface normal, for the Up, and 906 Km/s and the spin pointing at 60° from the surface normal, for the Alt. These speed values are larger than those of bulk semiconductors, such as CdSe and GaAs, thus making the hydrogenated graphene structures excellent candidates for spintronics applications.

PACS numbers:

I. INTRODUCTION

Spintronics is an emerging research field of electronics in which the manipulation and transport of spin of electrons in a solid state materials is central, adding a new degree of freedom to conventional charge manipulation.^{1,2} At present, there is an increasing interest in attaining the same level of control over the transport of spin at micro- or nano-scales, as it has been done for the flow of charge in typical 3D-bulk based electronic devices.³ Several semiconductor spintronics devices have been proposed^{4–7}, and some of them require spin polarized electrical current⁸ or pure spin current (PSC). One of the difficulties in creating measurable spin current and development of PSC based semiconductor devices is the fact that the spin relaxation time in conventional semiconducting materials is short to enable the spin transport, thus resulting in a non-observable spin current.⁹ For PSC there is no net motion of charge; spin-up electrons move in a given direction, while spin-down electrons travel in the opposite one. This effect can be due to one-photon absorption of linearly polarized light by a semiconductor, with filled valence bands and empty conduction bands, illuminated by light with photon energy larger than the energy gap. This phenomenon can be due to spin injection,¹⁰ Hall Effects,¹¹ interference of two optical beams,^{12,13} or one photon absorption of linearly polarized light¹⁴. The last effect has been observed in gallium arsenide (GaAs),^{15,16} aluminum-gallium arsenide (AlGaAs),¹⁶ and Co₂FeSi.¹⁷

The spin velocity injection (SVI) is an optical effect that quantifies the velocity at which a PSC moves along the direction $\hat{\mathbf{a}}$, with the spin of the electron polarized along the direction $\hat{\mathbf{b}}$. One photon absorption of polarized light produces an even distribution of electrons in \mathbf{k} space, regardless of the symmetry of the material, resulting in a null electrical current.¹⁴ Then, the electrons excited to the conduction bands at opposite \mathbf{k} points will result in opposite spin polarizations producing no net spin injection in centrosymmetric materials.¹⁴ If the crystalline structure of the material is noncentrosymmetric, the spin polarization injected at a given \mathbf{k} point not necessarily vanishes.^{36,37} Therefore, since the velocities of electrons at opposite \mathbf{k} points are opposite, a PSC will be produced.

Graphene, an allotrope of carbon with hexagonal 2D lattice structure, demonstrates properties such as fractional quantum Hall effect at room temperature, excellent thermal transport properties, excellent conductivity¹⁸ and strength^{19–22}, being a perfect platform for two-dimension (2D) electronic systems; however, most electronic applications are disabled by the absence of a semiconducting gap. Recent studies demonstrate that a narrow band gap can be opened in graphene by applying an electric field,²³ reducing the surface area,²⁴ or applying uniaxial strain.²⁵ Another possibility to open the gap is by doping; this has been successfully achieved using nitrogen,²⁶

boron-nitrogen,²⁷ silicon,²⁸ noble-metals,²⁹ and hydrogen.^{30–32} Depending on the percentage of hydrogenation and spatial arrangements of the hydrogen-carbon bonds, hydrogenated graphene demonstrates different structural configurations and a tunable electron gap, as it has been proven in Ref. 33. In this paper, we present two 50% hydrogenated graphene noncentrosymmetric structures, both presenting a discernible band gap. The first one, labelled as the Up structure, also known as graphone,³⁴ has hydrogen atoms bonded to the carbon layer only on the upper side of the structure; we consider here the magnetic isomer of graphone, with the so-called “chair” structure shown in Fig. 1. In contrast, the Alt structure, shown in Fig. 2, has hydrogen alternating on the upper and bottom sides of the carbon sheet.³⁵

Both the Up and the Alt structures are noncentrosymmetric, and therefore, they are good candidates in which SVI can be induced. In this article, we address theoretically the SVI by one-photon absorption of linearly polarized light, analyzing in our structures, two possible scenarios of practical interest. The first case is by fixing the spin of the electrons along z , i.e. perpendicular to the surface plane, with the resulting velocity directed along the surface of the structures in the xy plane. In the second case we fix the SVI velocity along the x or y direction, and then, the resulting spin is directed outward of the xy plane.

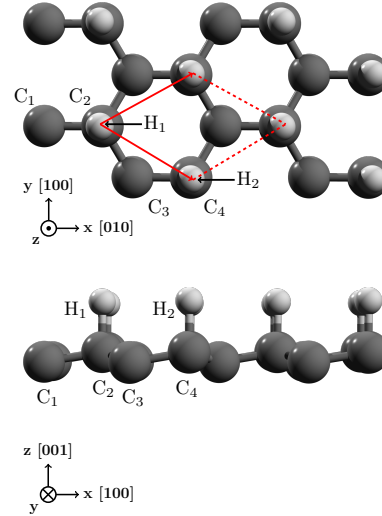


FIG. 1: Top (top panel) and side (bottom panel) views of the Up structure along with the Cartesian x , y , and z directions. The dark (light) spheres are the C (H) atoms. The primitive hexagonal unit cell is also shown. Anatoli: we are confused about the primitive hexagonal unit cell shown. For instance, according to us, if we take C_2 and apply the red arrow, it will end up in the site of C_4 , but these C atoms according to Table I are not equivalent, or are they?

This paper is organized as follows. In Section II we present the formalism and the main expres-

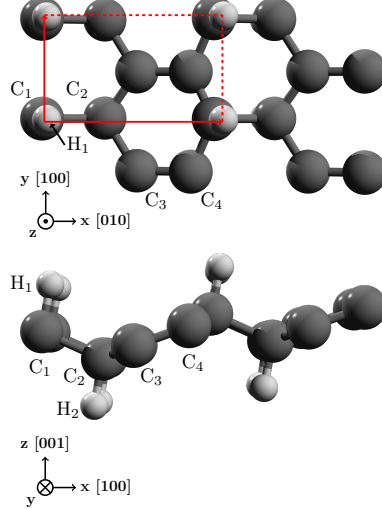


FIG. 2: Top (top panel) and side (bottom panel) views of the Alt structure along with the Cartesian x , y , and z directions. The dark (light) spheres are the C (H) atoms. The primitive hexagonal unit cell is also shown.

sions that describe PSC and SVI. In Section III we describe the numerical details and discuss the corresponding SVI spectra for the Up and Alt structures. Finally, we summarize our findings in Section IV.

II. THEORY

In this section, we summarize the theoretical approach, involved in calculation of the spin velocity injection (SVI) resulting from the pure spin current (PSC).

The operator that describes the electronic SVI is written as

$$\hat{K}^{ab} = \frac{1}{2} (\hat{v}^a \hat{S}^b + \hat{S}^b \hat{v}^a), \quad (1)$$

where $\hat{\mathbf{v}} = [\hat{\mathbf{r}}, \hat{H}_0]/i\hbar$ is the velocity operator, with $\hat{\mathbf{r}}$ being the position operator and \hat{H}_0 the unperturbed ground state Hamiltonian; the Roman superscripts indicate Cartesian coordinates. To obtain the expectation value of \hat{K}^{ab} , we use the length gauge for the perturbing Hamiltonian, written as

$$\hat{H}_p = -e\hat{\mathbf{r}} \cdot \mathbf{E}(t), \quad (2)$$

where the applied electric field of the beam of light is given by

$$\mathbf{E}(t) = \mathbf{E}(\omega)e^{-i\omega t} + \mathbf{E}^*(\omega)e^{i\omega t}. \quad (3)$$

In order to calculate the response of the system to $\mathbf{E}(t)$, one needs to take into account the excited coherent superposition of the spin-split conduction bands inherent to the noncentrosymmetric semiconductors considered in this work. To include the coherence, we follow Ref. 39 and use a multiple scale approach that solves the equation of motion for the single particle density matrix $\rho_{mn}(\mathbf{k}; t)$, leading to

$$\frac{\partial \rho_{cc'}(\mathbf{k})}{\partial t} = \frac{e^2 E^a(\omega) E^{b*}(\omega)}{i\hbar^2} \sum_v r_{cv}^a(\mathbf{k}) r_{vc'}^b(\mathbf{k}) \left(\frac{1}{\omega - \omega_{c'v}(\mathbf{k}) - i\epsilon} - \frac{1}{\omega - \omega_{cv}(\mathbf{k}) + i\epsilon} \right), \quad (4)$$

where we assumed that the conduction bands c and c' are quasi-degenerate states, and we take $\epsilon \rightarrow 0$ at the end of the calculation. The spin-splitting of the valence (v) bands is very small, and is neglected throughout this work.³⁹ The matrix elements of any operator \mathcal{O} are given by $\mathcal{O}_{nm}(\mathbf{k}) = \langle n\mathbf{k} | \hat{\mathcal{O}} | m\mathbf{k} \rangle$, where $H_0|n\mathbf{k}\rangle = \hbar\omega_n(\mathbf{k})|n\mathbf{k}\rangle$ with $\hbar\omega_n(\mathbf{k})$ being the energy of the electronic band n at point \mathbf{k} in the irreducible Brillouin zone (IBZ), $|n\mathbf{k}\rangle$ is the Bloch state, and $\omega_{nm}(\mathbf{k}) = \omega_n(\mathbf{k}) - \omega_m(\mathbf{k})$. Using $\mathcal{O} = \text{Tr}(\hat{\rho}\hat{\mathcal{O}})$ for the expectation value of an observable \mathcal{O} , where Tr denotes the trace, we obtain

$$\mathcal{O} = \int \frac{d^3k}{8\pi^3} \sum_{cc'} \rho_{cc'}(\mathbf{k}) \mathcal{O}_{c'c}(\mathbf{k}), \quad (5)$$

where we used the closure relationship $\sum_n |n\mathbf{k}\rangle \langle n\mathbf{k}| = 1$, where n goes over all v and c states, and the fact that $\rho_{vn}(\mathbf{k}) = \rho_{nv}(\mathbf{k}) = 0$ for $n = c, c'$. Therefore, using Eqs. (4) and (5), the rate of change of \mathcal{O} , $\dot{\mathcal{O}} = \text{Tr}(\dot{\hat{\rho}}\hat{\mathcal{O}})$, is given by

$$\dot{\mathcal{O}} = \frac{e^2}{i\hbar^2} \int \frac{d^3k}{8\pi^3} \sum'_{cc'} \mathcal{O}_{c'c}(\mathbf{k}) r_{cv}^a(\mathbf{k}) r_{vc'}^b(\mathbf{k}) \left(\frac{1}{\omega - \omega_{c'v}(\mathbf{k}) - i\epsilon} - \frac{1}{\omega - \omega_{cv}(\mathbf{k}) + i\epsilon} \right) E^a(\omega) E^{b*}(\omega). \quad (6)$$

The prime symbol ' in the sum means that c and c' are quasi-degenerate states, and the sum only covers these states. Replacing $\hat{\mathcal{O}} \rightarrow \hat{K}^{ab}$, in the above expression, one can show that

$$\dot{K}^{ab}(\omega) = \mu^{abcd}(\omega) E^c(\omega) E^{d*}(\omega), \quad (7)$$

where repeated Cartesians upperscripts are summed, and

$$\mu^{abcd}(\omega) = \frac{\pi e^2}{\hbar^2} \int \frac{d^3k}{8\pi^3} \sum'_{vcv} \delta(\omega - \omega_{cv}(\mathbf{k})) \text{Re} \left[K_{cc'}^{ab}(\mathbf{k}) \left(r_{vc'}^c(\mathbf{k}) r_{cv}^d(\mathbf{k}) + (c \leftrightarrow d) \right) \right] \quad (8)$$

is the pseudotensor that describes the rate of change of the PSC process in semiconductors. To derive what we presented above we used $K_{nm}^{ab}(-\mathbf{k}) = K_{nm}^{ab*}(\mathbf{k})$ which follows from time-reversal invariance. Since $\mu^{abcd}(\omega)$ is real, we have that $\mu^{abcd}(\omega) = \mu^{abdc}(\omega)$. We point out that Eq. (8)

is identical to Eq. (3) of Bhat et al.,¹⁴ derived using the semiconductor optical Bloch equations. Using the closure relation,

$$K_{cc'}^{ab}(\mathbf{k}) = \frac{1}{2} \sum_{l=v,c} \left(v_{cl}^a(\mathbf{k}) S_{lc'}^b(\mathbf{k}) + S_{cl}^b(\mathbf{k}) v_{lc'}^a(\mathbf{k}) \right). \quad (9)$$

We define the spin velocity injection (SVI) as

$$\mathcal{V}^{ab}(\omega) \equiv \frac{\dot{K}^{ab}(\omega)}{(\hbar/2)\dot{n}(\omega)}, \quad (10)$$

which gives the velocity, along direction $\hat{\mathbf{a}}$, at which the spin moves in a polarized state along direction $\hat{\mathbf{b}}$. The carrier injection rate $\dot{n}(\omega)$ is written as³⁹

$$\dot{n}(\omega) = \xi^{ab}(\omega) E^c(\omega) E^{d*}(\omega) \quad (11)$$

where the tensor

$$\xi^{ab}(\omega) = \frac{2\pi e^2}{\hbar^2} \int \frac{d^3 k}{8\pi^3} \sum_{vc} r_{vc'}^a(\mathbf{k}) r_{cv}^b(\mathbf{k}) \delta(\omega - \omega_{cv}(\mathbf{k})), \quad (12)$$

is related to the imaginary part of the linear optical response tensor by $\text{Im}[\epsilon^{ab}(\omega)] = 2\pi\epsilon_0\hbar\xi^{ab}(\omega)$.

The function $\mathcal{V}^{ab}(\omega)$ allows us to quantify two very important aspects of PSC. On one hand, we can fix the spin direction along $\hat{\mathbf{b}}$ and calculate the resulting electron velocity. On the other hand, we can fix the velocity of the electron along $\hat{\mathbf{a}}$ and study the resulting direction along which the spin is polarized. To this end, the additional advantage of 2D structures, besides being noncentrosymmetric, is that we can use an incoming linearly polarized light at normal incidence, and use the direction of the polarized electric field to control $\mathcal{V}^{ab}(\omega)$. Indeed, writing $\mathbf{E}(\omega) = E_0(\omega)(\cos\alpha\hat{\mathbf{x}} + \sin\alpha\hat{\mathbf{y}})$, where α is the polarization angle, we obtain from Eq. (10) that

$$\mathcal{V}^{ab}(\omega, \alpha) = \frac{2}{\hbar\xi(\omega)} \left(\mu^{abxx}(\omega) \cos^2 \alpha + \mu^{abyy}(\omega) \sin^2 \alpha + \mu^{abxy}(\omega) \sin 2\alpha \right), \quad (13)$$

since for the structures chosen in this article, $\xi^{xx}(\omega) = \xi^{yy}(\omega) \equiv \xi(\omega)$, and $\xi^{xy}(\omega) = 0$. Next, we identify two options for $\mathcal{V}^{ab}(\omega)$.

A. Fixing the spin polarization

Analyzing the SVI, Eq. (13), we calculate the magnitude of the electron velocity along the plane of the structure, with the spin polarized along $\hat{\mathbf{b}}$ direction as

$$\mathcal{V}_{\sigma^b}(\omega, \alpha) \equiv \sqrt{[\mathcal{V}^{xb}(\omega, \alpha)]^2 + [\mathcal{V}^{yb}(\omega, \alpha)]^2}, \quad (14)$$

and define the angle at which the velocity is directed on the xy plane as

$$\gamma_{\sigma^b}(\omega, \alpha) = \tan^{-1} \left(\frac{\mathcal{V}^{yb}(\omega, \alpha)}{\mathcal{V}^{xb}(\omega, \alpha)} \right). \quad (15)$$

We also define two special angles

$$\gamma_{\sigma^b}^{\parallel}(\omega, \alpha) = \alpha, \quad (16)$$

and

$$\gamma_{\sigma^b}^{\perp}(\omega, \alpha) = \alpha \pm 90^\circ, \quad (17)$$

corresponding to the electron velocity being parallel or perpendicular to the incoming light polarization direction, respectively. The subscript σ^b denotes the spin along $\hat{\mathbf{b}}$.

B. Fixing the electron velocity.

Fixing the calculated velocity along $a = x$ or $a = y$, we define its corresponding magnitude as

$$\mathcal{V}_a(\omega, \alpha) \equiv \sqrt{[\mathcal{V}^{ax}(\omega, \alpha)]^2 + [\mathcal{V}^{ay}(\omega, \alpha)]^2 + [\mathcal{V}^{az}(\omega, \alpha)]^2}, \quad (18)$$

from where we see that the spin would be oriented in the xyz system of coordinates by the defined polar angle

$$\theta_a(\omega, \alpha) = \cos^{-1} \left(\frac{\mathcal{V}^{az}(\omega, \alpha)}{\mathcal{V}_a(\omega, \alpha)} \right), \quad 0 \leq \theta \leq \pi, \quad (19)$$

and an azimuthal angle

$$\varphi_a(\omega, \alpha) = \tan^{-1} \left(\frac{\mathcal{V}^{ay}(\omega, \alpha)}{\mathcal{V}^{ax}(\omega, \alpha)} \right), \quad 0 \leq \varphi \leq 2\pi. \quad (20)$$

III. RESULTS

We present the calculated results of $\mathcal{V}_{\sigma^b}(\omega, \alpha)$ and $\mathcal{V}_a(\omega, \alpha)$ for the Up and Alt structures, both noncentrosymmetric 2D carbon systems with 50% hydrogenation, which are differently structurally arranged. We remind that the Up structure has hydrogen atoms only on the upper side of the carbon sheet, while the Alt structure has alternating hydrogen atoms on the upper and bottom sides. We take the carbon lattice to be along the xy plane for both structures, and the carbon-hydrogen bonds are outward the plane, they are perpendicular to xz plane for the Up structure,

Atom	Position (Å)		
	x	y	z
type			
H ₁	-0.61516	-1.77416	0.73196
H ₂	0.61518	0.35514	0.73175
C ₁	-0.61516	-1.77264	-0.49138
C ₂	-0.61516	-0.35600	-0.72316
C ₃	0.61516	0.35763	-0.49087
C ₄	0.61518	1.77416	-0.73196

TABLE I: Atomic positions in the unit cell of the Up structure shown in Fig. 1.

Atom	Position (Å)		
	x	y	z
type			
H ₁	-0.61516	-1.42140	1.47237
C ₁	-0.61516	-1.73300	0.39631
C ₂	0.61516	1.73300	0.15807
C ₃	0.61516	0.42201	-0.15814
C ₄	-0.61516	-0.37396	-0.39632
H ₂	-0.61516	-0.68566	-1.47237

TABLE II: Atomic positions in the unit cell of the Alt structure shown in Fig. 2.

as depicted in Figs. 1, and off the normal for the Alt structure 2. The coordinates for the Up and Alt unit cells of the structures are presented in Tables I and II, respectively.

We calculated the self-consistent ground state and the Kohn-Sham states within density functional theory in the local density approximation (DFT-LDA), with a planewave basis using the ABINIT code⁴⁰. We used Hartwigsen- Goedecker-Hutter (HGH) relativistic separable dual-space Gaussian pseudopotentials⁴¹, including the spin-orbit interaction needed to calculate $\mu^{abcd}(\omega, \alpha)$ presented in Eq. (8). The convergence parameters for the calculations, corresponding to the Up and Alt structures are cutoff energies up to 65 Ha, resulting in LDA energy band gaps of 0.084 eV and 0.718 eV, respectively, and 14452 \mathbf{k} points in the IBZ where the energy eigenvalues and matrix elements were calculated; to integrate $\mu^{abcd}(\omega)$ and $\xi^{ab}(\omega)$ the linearized analytic tetrahedron method (LATM) has been used.³⁹ We neglect the anomalous velocity term $\hbar(\boldsymbol{\sigma} \times \nabla V)/4m^2c^2$, where V is the crystal potential, in $\hat{\mathbf{v}}$ of Eq. (1), as this term is known to give small contribution to PSC.¹⁴ Therefore, $[\hat{\mathbf{v}}, \hat{\mathbf{S}}] = 0$, and Eq. (1) reduces to $\hat{K}^{ab} = \hat{v}^a \hat{S}^b = \hat{S}^b \hat{v}^a$. Finally, the prime

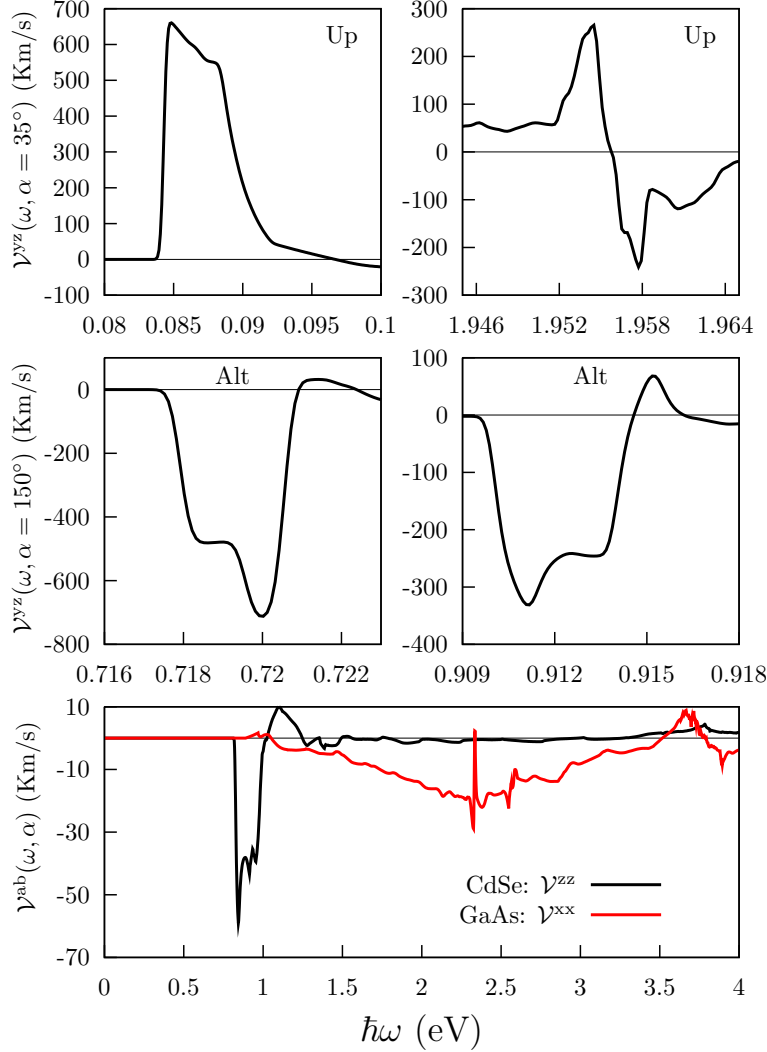


FIG. 3: $\mathcal{V}^{ab}(\omega, \alpha)$ vs. $\hbar\omega$, for the angles α that maximize the signal. The largest velocity are at the low energy regions of the spectra for the Alt and Up structures, becoming different from zero at the energy gap of each structure. In the high energy regions, the values of $\mathcal{V}^{ab}(\omega, \alpha)$ are also very large compared to the 3D case of CdSe and GaAs, shown at the bottom panel.

in the sum of Eq. (8) is restricted to quasi-degenerated conduction bands c and c' that are closer than 30 meV, which is both typical laser- pulse energy width and the thermal room-temperature energy level broadening.³⁹

A. SVI: Spin velocity injection

In Fig. 3, we show $\mathcal{V}^{ab}(\omega, \alpha)$ vs. $\hbar\omega$ for the velocity and spin directions $\hat{\mathbf{a}}$ and $\hat{\mathbf{b}}$, and for the angle α , at which the signal is maximized, for the Up and Alt structures, and for CdSe and GaAs

bulk systems, shown for comparison. As expected from Eq. (8), $\mathcal{V}^{ab}(\omega, \alpha)$ becomes different from zero right at the corresponding energy gap of each system. For the 2D structures considered, the spectrum contains two narrow energy regions with strong response, while for the bulk systems, the spectra covers a rather wide energy range, but with a much weaker response. For the Up structure, at $ab = yz$ and $\alpha = 35^\circ$ the response is maximized, which means that an incoming light with its electric field polarized at 35° from the x direction will induce electrons to move along y , parallel to the surface, with their spin polarized along z , perpendicular to the surface. The corresponding speeds are the following: Right at the energy onset, $\mathcal{V}^{yz}(\omega, \alpha) = 668 \text{ Km/s}$, remains almost constant for 65 meV, and then decreases to zero. A second region with high velocity is above 1.946 eV with two, opposite in sign, maxima of the speed: $\mathcal{V}^{yz}(\omega, \alpha) = 266.3 \text{ Km/s}$ at $\hbar\omega = 1.954 \text{ eV}$, and $\mathcal{V}^{ab}(\omega, \alpha) = -241.4 \text{ Km/s}$ at $\hbar\omega = 1.958 \text{ eV}$; a positive (negative) $\mathcal{V}^{ab}(\omega, \alpha)$ means that the electrons move parallel (antiparallel) to the electric field. Likewise, for the Alt structure, we also find that $ab = yz$ and $\alpha = 150^\circ$ maximizes the response, where two extreme values of \mathcal{V}^{yz} are found, one at $\hbar\omega = 0.720 \text{ eV}$ of $\mathcal{V}^{yz} = -711.9 \text{ Km/s}$, and the other at $\hbar\omega = 0.911 \text{ eV}$ of $\mathcal{V}^{yz} = -330.6 \text{ Km/s}$.

For the bulk structures, we calculate $\mathcal{V}^{ab}(\omega)$ from Eq. (10) by simply using $\boldsymbol{\mu}_{\max}$. For CdSe, we find that for $\hbar\omega = 0.844 \text{ eV}$, $\boldsymbol{\mu}_{\max} \rightarrow \mu^{zzzz}$, and $\mathcal{V}^{zz}(\omega) = -59.0 \text{ Km/s}$, and for GaAs at $\hbar\omega = 2.324 \text{ eV}$, $\boldsymbol{\mu}_{\max} \rightarrow \mu^{aaaa}$ and $\mathcal{V}^{aa}(\omega, \alpha) = -28.7 \text{ Km/s}$, with $a = x, y, z$. For these bulk semiconductors, the x , y , and z axis are taken along the standard cubic unit cell directions, [100], [010], and [001], respectively. In Table III, we compare $\mathcal{V}^{ab}(\omega, \alpha)$ for the 2D structures considered and bulk crystals. We stress that, as shown in the figure, for the 2D structures have maxima in $\mathcal{V}^{ab}(\omega; \alpha)$ are higher than for the bulk crystals. In particular, the Alt structure demonstrates a $\mathcal{V}^{ab}(\omega; \alpha)$ more than ten times larger than that of CdSe and GaAs.

B. Fixing spin

In this subsection, we calculate $\mathcal{V}_{\sigma^z}(\omega, \alpha)$, Eq. (14), for the case with the spin fixed along z , i.e. directed perpendicularly to the surface of the Up and Alt structures. Also, we calculate $\gamma_{\sigma^z}(\omega, \alpha)$ from Eq. (15), which determines the direction of the injected electrons movement along the surface of each structure. We mention that we have also analyzed the cases when the spin is directed along x or y , finding similar qualitative results to those presented below.

Structure	System type	Pol. Ang.	Energy [eV]	$\mathcal{V}^{ab}(\omega, \alpha)$	
				ab	[Km/s]
Up	2D	35	0.084	yz	660.5
			1.954	yz	266.3
			1.958	yz	-241.4
Alt	2D	150	0.720	yz	-711.9
			0.911	yz	-330.6
CdSe	bulk	-	0.844	zz	-59.0
GaAs	bulk	-	2.324	xx	-28.7

TABLE III: Comparison of the reported maximum values of $\mathcal{V}^{ab}(\omega, \alpha)$ for the different structures and their corresponding polarization angle α and energy $\hbar\omega$.

1. Up structure

In the top panel of Fig. 4, we plot $\mathcal{V}_{\sigma^z}(\omega, \alpha)$ vs. $0.080 \text{ eV} \leq \hbar\omega \leq 0.096 \text{ eV}$ (similar energy range for the Up structure shown in the left panel of Fig. 3 and $0^\circ \leq \alpha \leq 180^\circ$. We see a broad peak that reaches the maximum of $\mathcal{V}_{\sigma^z}(\omega, \alpha) = 739.7 \text{ Km/s}$ at $\alpha = 35^\circ$ and $\hbar\omega = 0.084 \text{ eV}$, The variation of $\mathcal{V}_{\sigma^z}(\omega, \alpha)$ as a function of α , which comes from the interplay of the μ tensor components as multiplied by the trigonometric functions of Eq. (13), gives a sizable set of values between 739.7 Km/s and 165.4 Km/s, for $0.084 \text{ eV} \leq \hbar\omega \leq 0.090 \text{ eV}$. In the bottom panel, we show $\mathcal{V}_{\sigma^z}(\omega, \alpha)$ vs. α (left scale, black line), at $\hbar\omega = 0.084 \text{ eV}$, thus following the ridge in the 3D plot of the top panel. Also, we plot the corresponding velocity angle $\gamma_{\sigma^z}(\omega, \alpha)$ (right scale, red line), where it is very interesting to see that $\gamma_{\sigma^z}(\omega, \alpha)$ is centered at 64.55° with a rather small deviation of only $\pm 0.03^\circ$, for the whole range of α . This result means that for $\hbar\omega = 0.084 \text{ eV}$ and for all values of α , the electrons, with the chosen spin pointing along z , will move at the angle of $\gamma_{\sigma^z}(\omega, \alpha) \sim 64.5^\circ$ with respect to the x direction, with the range of high speeds $\mathcal{V}_{\sigma^z}(\omega, \alpha)$ shown in the figure. Also, from Eq. (16) we find that $\gamma_{\sigma^z}^{\parallel}(\omega, \alpha) = \alpha = 64.56^\circ$, with $\mathcal{V}_{\sigma^z}(\omega, \alpha) = 631.1 \text{ Km/s}$ (see green arrow), and that from Eq. (17), $\gamma_{\sigma^z}^{\perp}(\omega, \alpha) = \alpha - 90^\circ = 64.50^\circ$, gives $\alpha = 154.50^\circ$, with $\mathcal{V}_{\sigma^z}(\omega, \alpha) = 191.5 \text{ Km/s}$ (see blue arrow). Thus, at $\hbar\omega = 0.084 \text{ eV}$, an incident field, polarized at $\alpha \sim 65.5^\circ$ or $\sim 154.5^\circ$, injects electrons with their spin polarized along z , which move parallel or perpendicular to the incident electric field, with a speed of 631.14 Km/s or 191.5 Km/s, respectively.

Now, we analyze the results for the second energy range of the Up structure shown in Fig. 3. In the top panel of Fig. 5, we plot $\mathcal{V}_{\sigma^z}(\omega, \alpha)$ vs. $1.950 \text{ eV} \leq \hbar\omega \leq 1.960 \text{ eV}$ and $0^\circ \leq \alpha \leq 180^\circ$. We see two broad peaks that maximize at $\alpha = 35^\circ$ and $\hbar\omega = 1.954 \text{ eV}$, with a value of $\mathcal{V}_{\sigma^z}(\omega, \alpha) =$

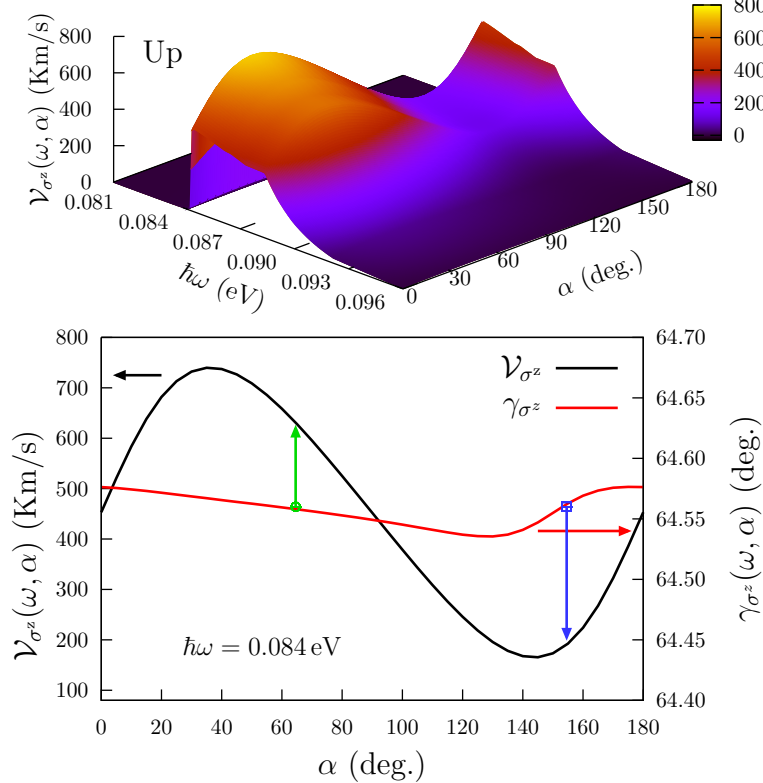


FIG. 4: Color online. For the Up structure, the top panel shows $V_{\sigma^z}(\omega, \alpha)$ vs. $\hbar\omega$ and α , and the bottom panel shows $\gamma_{\sigma^z}(\omega, \alpha)$ (right scale, red line), and $V_{\sigma^z}(\omega, \alpha)$ (left scale, black solid line), vs. α , for $\hbar\omega = 0.084$ eV, i.e. along the ridge shown in the 3D plot.

193.5 Km/s, and at $\alpha = 35^\circ$ and $\hbar\omega = 1.957$ eV, with a value of $V_{\sigma^z}(\omega, \alpha) = 170.6$ Km/s. We only analyze the highest maximum in the bottom panel, where we show $V_{\sigma^z}(\omega, \alpha)$ vs. α (left scale, black line), at $\hbar\omega = 1.954$ eV, thus following the highest ridge shown in the 3D plot of the top panel. Also, we plot the corresponding velocity angle $\gamma_{\sigma^z}(\omega, \alpha)$ (right scale, red line), where in this case we see that the values of $\gamma_{\sigma^z}(\omega, \alpha)$ have more dispersion, as a function of α , than for the lower energy range shown in the bottom panel of Fig. 4. However, $\gamma_{\sigma^z}(\omega, \alpha) \sim 77.8^\circ$ is nearly constant from $\alpha = 0^\circ$ up to $\alpha \sim 85^\circ$. In this case, we find that $\gamma_{\sigma^z}^{\parallel}(\omega, \alpha) = \alpha = 78.0^\circ$, with $V_{\sigma^z}(\omega, \alpha) = 115.0$ Km/s (as indicated by green arrow), and that from Eq. (17), $\gamma_{\sigma^z}^{\perp}(\omega, \alpha) = \alpha - 90^\circ = 167.8^\circ$, gives $\alpha = 77.8^\circ$, with $V_{\sigma^z}(\omega, \alpha) = 65.6$ Km/s (see blue arrow). Thus, through the correct choice of $\hbar\omega$ and α we could inject electrons, in this case with their spin polarized along z , which move parallel or perpendicular to the incident electric field, with sizable speeds.

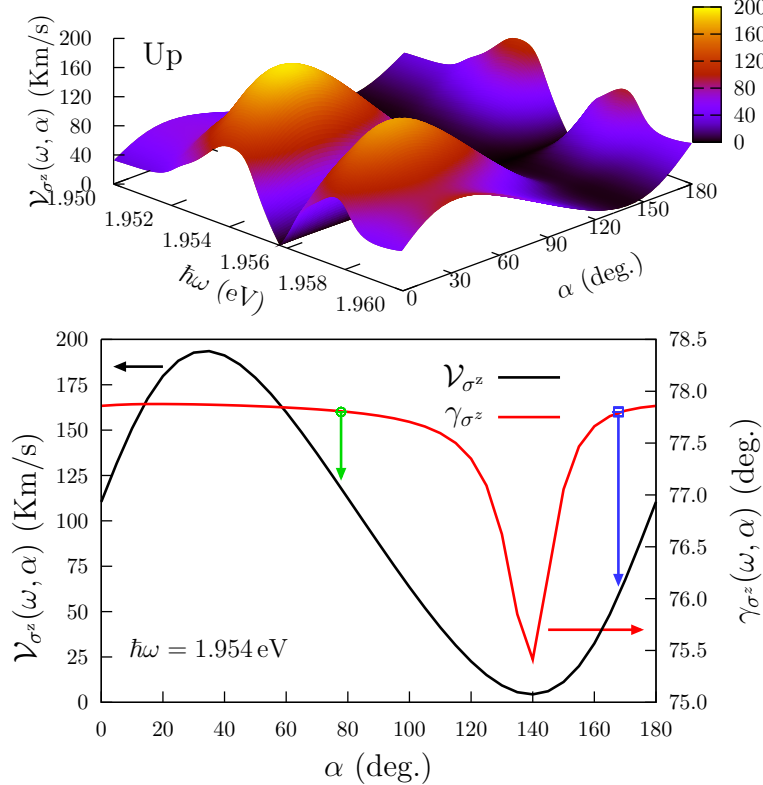


FIG. 5: For the Up structure, the top panel shows $V_{\sigma^z}(\omega, \alpha)$ vs. $\hbar\omega$ and α , and the bottom panel shows $\gamma_{\sigma^z}(\omega, \alpha)$ (right scale, red line, long dashes), and $V_{\sigma^z}(\omega, \alpha)$ (left scale, black solid line), vs. α , for $\hbar\omega = 1.954$ eV, i.e. along the highest ridge shown in the 3D plot.

2. Alt structure

We proceed to analyze the Alt structure, just as we did with the Up structure, but in this case, we only choose the lower energy range shown in the left central panel of Fig. 3. In the top panel of Fig. 6, we plot $V_{\sigma^z}(\omega, \alpha)$ vs. $0.715 \text{ eV} \leq \hbar\omega \leq 0.725 \text{ eV}$ and $0^\circ \leq \alpha \leq 180^\circ$. We see a broad peak that maximizes at $\alpha = 150^\circ$ and $\hbar\omega = 0.720 \text{ eV}$, with a value of $V_{\sigma^z}(\omega, \alpha) = 644.9 \text{ Km/s}$. In the bottom panel, we show $V_{\sigma^z}(\omega, \alpha)$ vs. α (left scale, black line), at $\hbar\omega = 0.720 \text{ eV}$, thus following the highest ridge shown in the 3D plot of the top panel. Also, we plot the corresponding velocity angle $\gamma_{\sigma^z}(\omega, \alpha)$ (right scale, red line), where now we see that $\gamma_{\sigma^z}(\omega, \alpha)$ is centered at 109.2° having variations of $\pm 1.0^\circ$ for $0^\circ \leq \alpha \leq 180^\circ$. In this case, we find that $\gamma_{\sigma^z}^{\parallel}(\omega, \alpha) = \alpha = 108.8^\circ$, with $V_{\sigma^z}(\omega, \alpha) = 450.05 \text{ Km/s}$ (see green arrow), and that from Eq. (17), $\gamma_{\sigma^z}^{\perp}(\omega, \alpha) = \alpha - 90^\circ = 110.0^\circ$, gives $\alpha = 20.0^\circ$, with $V_{\sigma^z}(\omega, \alpha) = 60.84 \text{ Km/s}$ (see blue arrow). Thus, as for the Up structure, we could inject electrons with a fixed spin, which moves parallel or perpendicular to the incident electric field.

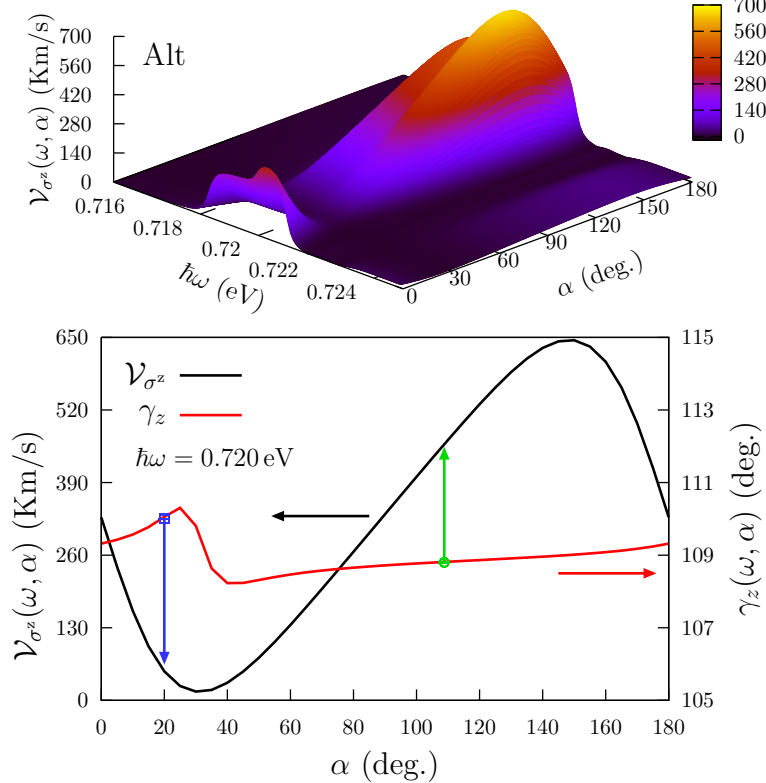


FIG. 6: Color online. For the Alt structure, the top panel shows $\mathcal{V}_{\sigma^z}(\omega, \alpha)$ vs. $\hbar\omega$ and α , and the bottom panel shows $\gamma_z(\omega, \alpha)$ (right scale, red line), and $\mathcal{V}_{\sigma^z}(\omega, \alpha)$ (left scale, black line), vs. α , for $\hbar\omega = 0.720$ eV, i.e. along the ridge shown in the 3D plot.

C. Fixing the electron velocity

Here we calculated $\mathcal{V}_a(\omega, \alpha)$ (Eq. (18)) after fixing the electron velocity direction, $\hat{\mathbf{a}}$, to the x or y direction along the surface of the Up and Alt structures. From Eqns. (19) and (20), we determined the corresponding polar angle, $\theta_a(\omega, \alpha)$, and azimuthal angle, $\varphi_a(\omega, \alpha)$.

1. Up structure

For the Up structure, we find once again that $\alpha = 35^\circ$ maximizes the response. In Fig. 7, we plot $\mathcal{V}_a(\omega, \alpha)$ (left scale, black line), $\theta_a(\omega, \alpha)$ (right scale, red line), and $\varphi_a(\omega, \alpha)$, (right scale, blue line), vs. $\hbar\omega$, for $a = x, y$. We see that for $\hbar\omega = 0.084$ eV, the response has a maximum of $\mathcal{V}_x(\omega, \alpha) = 431.7$ Km/s at $\theta_x(\omega, \alpha) = 42.5^\circ$, and $\varphi_x(\omega, \alpha) = 208.3^\circ$, and $\mathcal{V}_y(\omega, \alpha) = 687.9$ Km/s at $\theta_y(\omega, \alpha) = 13.9^\circ$, and $\varphi_y(\omega, \alpha) = 82.1^\circ$. This means that the spin is directed upward the third quadrant of the xy plane when the electron moves along x , and is almost parallel to the xy plane

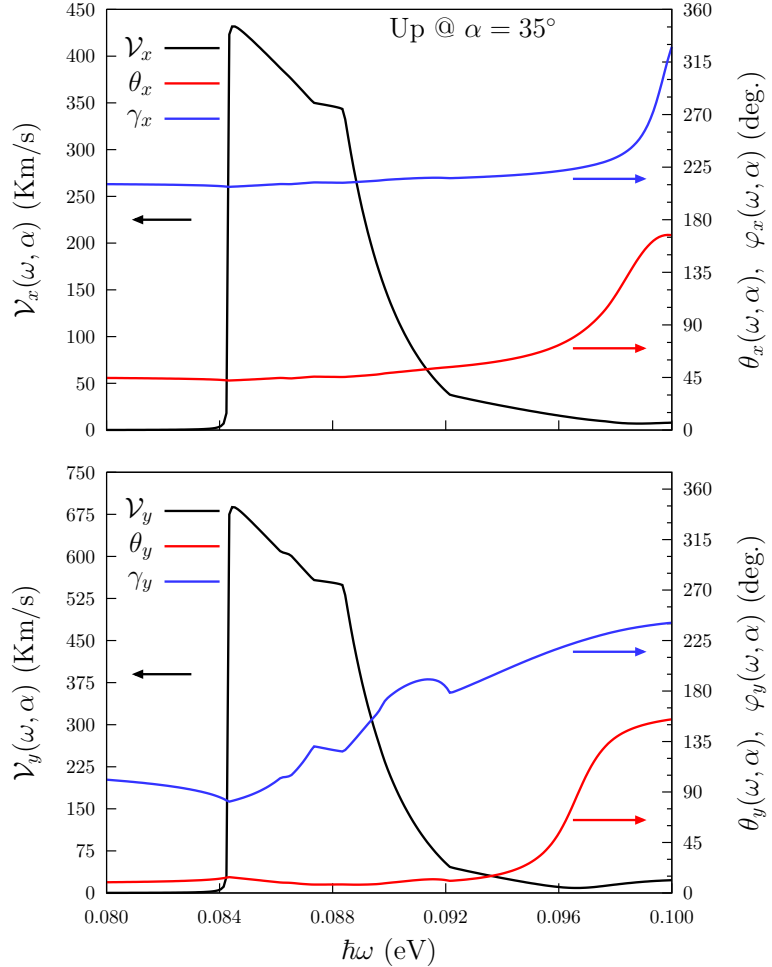


FIG. 7: For the Up structure we show the velocity $\mathcal{V}_a(\omega, \alpha)$ (left scale, black line), the polar angle $\theta_a(\omega, \alpha)$ (right scale, red line), and the azimuthal angle $\varphi_a(\omega, \alpha)$, (right scale, blue line), *vs.* $\hbar\omega$, for $\alpha = 35^\circ$, and $a = x$ and $a = y$.

in the first quadrant when it moves along y . Also from this figure, we see that when the electron moves along x , the spin direction is almost constant for all the energies across the peak of the response, having $42.5^\circ < \theta_x(\omega, \alpha) < 53.7^\circ$ and $208.3^\circ < \varphi_x(\omega, \alpha) < 215.7^\circ$. When the electron moves along y , the spin polar angle has again small variations, $11.3^\circ < \theta_y(\omega, \alpha) < 13.9^\circ$, but the azimuthal angle varies significantly, $82.1^\circ < \varphi_y(\omega, \alpha) < 182.4^\circ$.

In Fig. 8, we plot $\mathcal{V}_a(\omega, \alpha)$ *vs.* $\hbar\omega$, in the range where there two local maxima with opposite sign at $\hbar\omega = 1.954$ eV and $\hbar\omega = 1.957$ eV occur. The first is the largest of the two, with $\mathcal{V}_x(\omega, \alpha) = 61.2$ Km/s, $\theta_x(\omega, \alpha) = 48.3^\circ$, and $\varphi_x(\omega, \alpha) = 54.3^\circ$, for the electron moving along x ; and $\mathcal{V}_y(\omega, \alpha) = 293.2$ Km/s, $\theta_y(\omega, \alpha) = 49.8^\circ$, and $\varphi_y(\omega, \alpha) = 51.9^\circ$ for the electron moving along y . For the peak at $\hbar\omega = 1.957$ eV, we obtain $\theta_x(\omega, \alpha) = 129.8^\circ$ and $\varphi_x(\omega, \alpha) = 231.7^\circ$, with $\mathcal{V}^x(\omega, \alpha) = 54.6$ Km/s and $\theta_y(\omega, \alpha) = 129.3^\circ$; and $\varphi_y(\omega, \alpha) = 230.7^\circ$, with $\mathcal{V}^y(\omega, \alpha) = 263.7$ Km/s. We remark that these

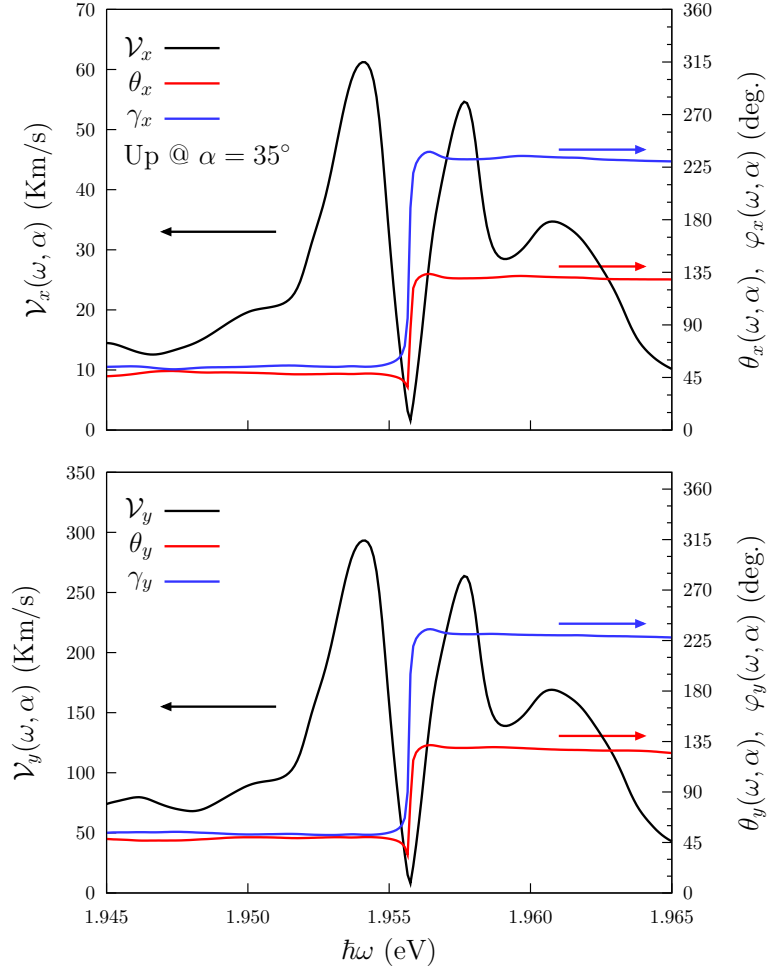


FIG. 8: For the Up structure we show the spin velocity $\mathcal{V}_a(\omega, \alpha)$ (left scale, black line), the polar angle $\theta_a(\omega, \alpha)$ (right scale, red line), and the azimuthal angle $\varphi_a(\omega, \alpha)$, (right scale, blue line), vs. $\hbar\omega$, for $\alpha = 35^\circ$, and $a = x$ or $a = y$.

angles are almost constant for all the energy values across the peak of these two local maxima, for which the spin is directed upward in the first quadrant of the xy plane when the electron moves along either x or y directions.

2. Alt structure

In Figs. 9 and 10, we plot $\mathcal{V}_a(\omega, \alpha)$ (left scale, black line), $\theta_a(\omega, \alpha)$ (right scale, red line), and $\varphi_a(\omega, \alpha)$, (right scale, blue line), vs. $\hbar\omega$ in two different ranges, and for $a = x, y$. In this case, $\alpha = 150^\circ$ maximizes both $\mathcal{V}_x(\omega, \alpha)$ and $\mathcal{V}_y(\omega, \alpha)$, as a function of α . In Fig. 9, the absolute maximum $\mathcal{V}_x(\omega, \alpha) = 301.7$ Km/s is at $\hbar\omega = 0.720$ eV, $\theta_x(\omega, \alpha) = 44.5^\circ$ and $\varphi_x(\omega, \alpha) = 51.2^\circ$, and $\mathcal{V}_y(\omega, \alpha) = 905.6$ Km/s at $\theta_y(\omega, \alpha) = 119.7^\circ$ and $\varphi_y(\omega, \alpha) = 163.4^\circ$. Thus, the spin is directed

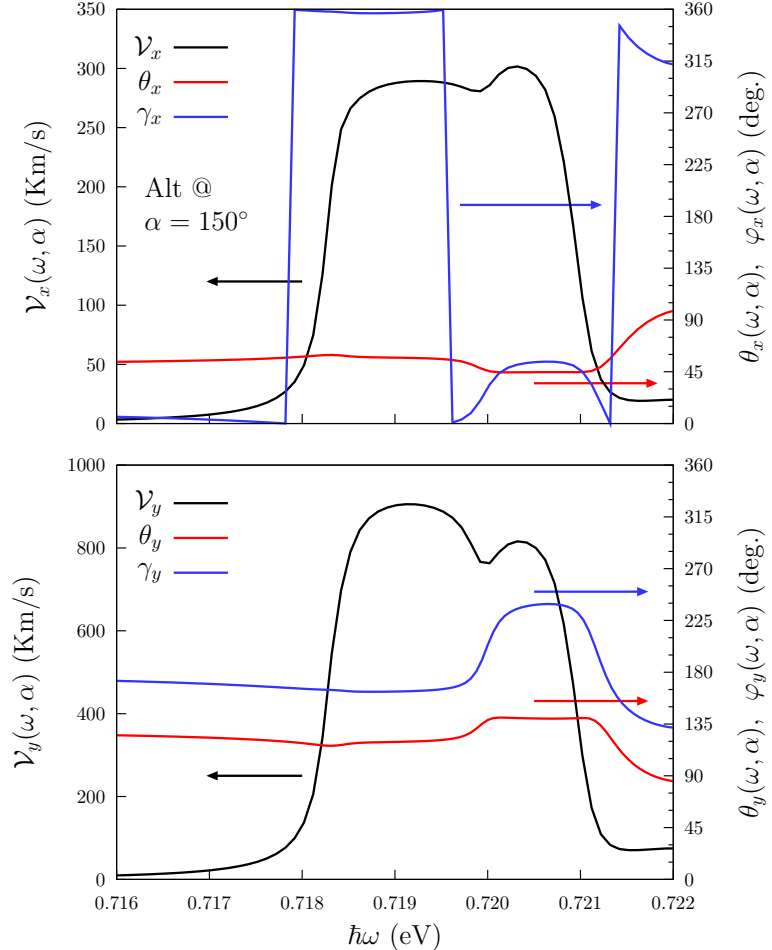


FIG. 9: For the Alt structure we show the velocity $\mathcal{V}_a(\omega, \alpha)$ (left scale, black line), the polar angle $\theta_a(\omega, \alpha)$ (right scale, red line), and the azimuthal angle $\varphi_a(\omega, \alpha)$, (right scale, blue line), *vs.* $\hbar\omega$, for $\alpha = 150^\circ$, and $a = x$ or $a = y$.

upward the fourth quadrant of the xy plane when the spin velocity is directed along x , while it is directed downward the second quadrant when the spin velocity is directed along y . Finally, in Fig. 10, the absolute maximum is at $\hbar\omega = 0.911$ eV at $\mathcal{V}_x(\omega, \alpha) = 276.3$ Km/s, $\theta_x(\omega, \alpha) = 154.6^\circ$, and $\varphi_x(\omega, \alpha) = 292.3^\circ$, and $\mathcal{V}_y(\omega, \alpha) = 468.6$ Km/s at $\theta_y(\omega, \alpha) = 129.2^\circ$, and $\varphi_y(\omega, \alpha) = 228.3^\circ$, implying that the spin is directed downward the fourth quadrant of the xy plane when the spin velocity is directed along x , while is directed downward the third quadrant when the spin velocity is directed along y .

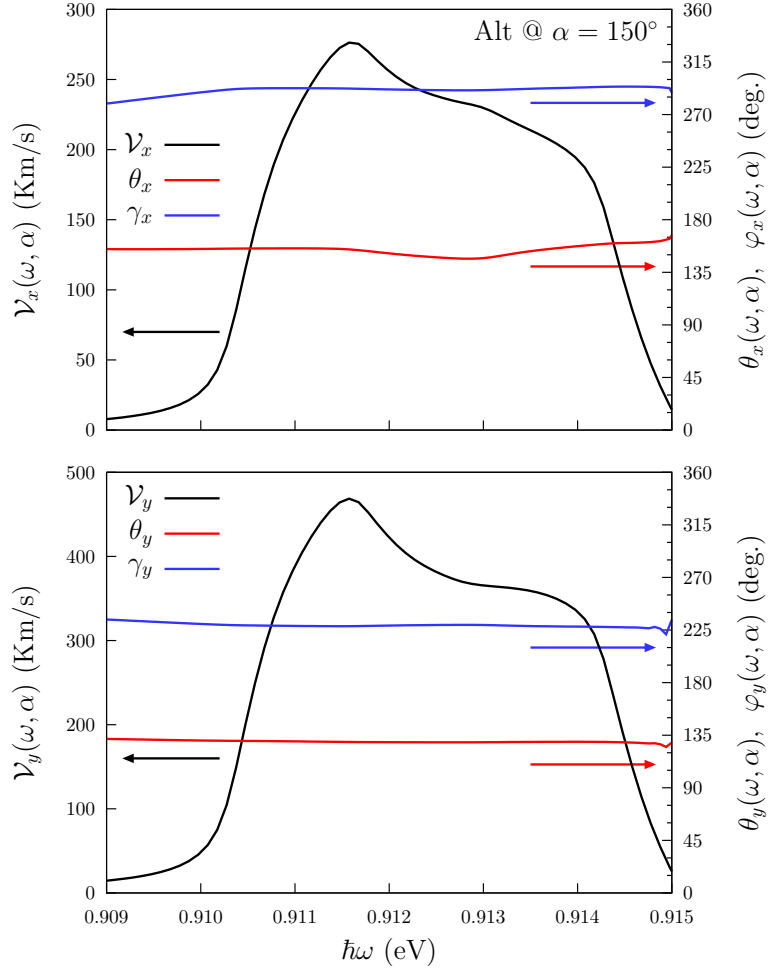


FIG. 10: For the Alt structure we show $\mathcal{V}_a(\omega, \alpha)$ (left scale, black line), the polar angle $\theta_a(\omega, \alpha)$ (right scale, red line), and the azimuthal angle $\varphi_a(\omega, \alpha)$, (right scale, blue line), *vs.* $\hbar\omega$, for $\alpha = 150^\circ$, and $a = x$ or $a = y$.

IV. CONCLUSIONS

We reported the results of an *ab initio* calculations for the spin velocity injection (SVI) due to the one-photon absorption of the linearly polarized light in the Up and Alt 2D 50% hydrogenated graphene structures. Different possible arrangements of the spin injection have been considered: we made the calculations for the cases when the spin is polarized in z direction or when the velocity is directed along x or y . To the best of our knowledge, this effect has not been previously reported in this 2D partially hydrogenated structures. We have shown that the SVI demonstrates an anisotropic behavior, which is very sensitive to the symmetry of the structures of interest. We have found that the Up structure shows the strongest response for the spin directed along z , resulting in the velocity $\mathcal{V}_{\sigma^z}(\omega, \alpha) = 668.0$ Km/s for the incoming photon energy of 0.084 eV. Also,

the Alt structure has the strongest response when the spin moves along y direction, resulting in $\mathcal{V}^y(\omega, \alpha) = 905.6$ Km/s for the incoming photon energy of 0.720 eV. The speed values obtained here are of the same order of magnitude as those of Ref. 13 in unbiased semiconductor quantum well structures, while they are of order of magnitude higher compared to 3D bulk materials. The spin relaxation time in pure and doped graphene is long enough in the order from nanoseconds to milliseconds.^{42,43} Therefore, according to our results, due to the high spin velocity transport both structures considered are the excellent candidates for the development of spintronics devices that require pure spin current (PSC).

V. ACKNOWLEDGMENT

This work has been supported by *Consejo Nacional de Ciencia y Tecnología* (CONACyT), México, Grant No. 153930. R.Z.P. thanks CONACyT for scholarship support.

- ¹ S. A. Wolf, D. D. Awschalom, R. A. Buhrman, J. M. Daughton, S. Von Molnar, M. L. Roukes, A. Y. Chtchelkanova, and D. M. Treger, *Science* **294**, 1488 (2001).
- ² J. Fabian, A. Matos-Abiague, C. Ertler, P. Stano, and I. Zutic, *Ac. Phys. Slov.* (2007).
- ³ D. D. Awschalom and M. E. Flatté, *Nat. Phys.* **3**, 153 (2007).
- ⁴ S. Majumdar, R. Laiho, P. Laukkanen, I. J. Väyrynen, H. S. Majumdar, and R. Österbacka, *App. Phys. Lett.* **89**, 122114 (2006).
- ⁵ S. Datta and B. Das, *App. Phys. Lett.* **56**, 665 (1990).
- ⁶ M. Götte, M. Joppe, and T. Dahm, *Scientific Reports* **6** (2016).
- ⁷ Y. V. Pershin and M. Di Ventra, *Phys. Rev. B* **78**, 113309 (2008).
- ⁸ D. D. Awschalom, D. Loss, and N. Samarth, *Semiconductor Spintronics and Quantum Computation* (Springer Science & Business Media, 2013).
- ⁹ S. Murakami, N. Nagaosa, and S. C. Zhang, *Science* **301**, 1348 (2003).
- ¹⁰ A. Malshukov, C. Tang, C. Chu, and K.-A. Chao, *Phys. Rev. B* **68**, 233307 (2003).
- ¹¹ J. Sinova, D. Culcer, Q. Niu, N. A. Sinitsyn, T. Jungwirth, and A. H. MacDonald, *Phys. Rev. Lett.* **92**, 126603 (2004).
- ¹² R. D. R. Bhat and J. E. Sipe, *Phys. Rev. Lett.* **85**, 5432 (2000).
- ¹³ A. Najmaie, R. D. R. Bhat, and J. E. Sipe, *Phys. Rev. B* **68**, 165348 (2003).
- ¹⁴ R. D. R. Bhat, F. Nastos, A. Najmaie, and J. E. Sipe, *Phys. Rev. Lett.* **94**, 096603 (2005).
- ¹⁵ H. Zhao, E. J. Loren, H. M. Van Driel, and A. L. Smirl, *Phys. Rev. lett.* **96**, 246601 (2006).

- ¹⁶ M. J. Stevens, A. L. Smirl, R. D. R. Bhat, A. Najmaie, J. E. Sipe, and H. M. Van Driel, Phys. Rev. Lett. **90**, 136603 (2003).
- ¹⁷ T. Kimura, N. Hashimoto, S. Yamada, M. Miyao, and K. Hamaya, NPG Asia Mat. **4**, e9 (2012).
- ¹⁸ H. B. Heersche, P. Jarillo-Herrero, J. B. Oostinga, L. M. K. Vandersypen, and A. F. Morpurgo, Nature **446**, 56 (2007).
- ¹⁹ A. Geim and K. Novoselov, Nat. Mater. **6**, 183 (2007).
- ²⁰ A. Reina, X. Jia, J. Ho, D. Nezich, H. Son, V. Bulovic, M. Dresselhaus, and J. Kong, Nano Lett. **9**, 30 (2008).
- ²¹ K. S. Novoselov, Z. Jiang, Y. Zhang, S. V. Morozov, H. L. Stormer, U. Zeitler, J. C. Maan, G. S. Boebinger, P. Kim, and A. K. Geim, Science **315**, 1379 (2007).
- ²² A. Balandin, S. Ghosh, W. Bao, I. Calizo, D. Teweldebrhan, F. Miao, and C. Lau, Nano Lett. **8**, 902 (2008).
- ²³ Y. Zhang, T. Tang, C. Girit, Z. Hao, M. Martin, A. Zettl, M. Crommie, Y. Shen, and F. Wang, Nature **459**, 820 (2009).
- ²⁴ M. Han, B. Özyilmaz, Y. Zhang, and P. Kim, Phys. Rev. Lett. **98**, 206805 (2007).
- ²⁵ Z. Ni, T. Yu, Y. Lu, Y. Wang, Y. P. Feng, and Z. Shen, ACS Nano **2**, 2301 (2008).
- ²⁶ D. Wei, Y. Liu, Y. Wang, H. Zhang, L. Huang, and G. Yu, Nano lett. **9**, 1752 (2009).
- ²⁷ B. Guo, L. Fang, B. Zhang, and J. R. Gong, Ins. J. **1**, 80 (2011).
- ²⁸ C. Coletti, C. Riedl, D. S. Lee, B. Krauss, L. Patthey, K. von Klitzing, J. H. Smet, and U. Starke, Phys. Rev. B **81**, 235401 (2010).
- ²⁹ A. Varykhalov, M. R. Scholz, T. K. Kim, and O. Rader, Phys. Rev. B **82**, 121101 (2010).
- ³⁰ D. C. Elias, R. R. Nair, T. M. G. Mohiuddin, S. V. Morozov, P. Blake, M. P. Halsall, A. C. Ferrari, D. W. Boukhvalov, M. I. Katsnelson, A. K. Geim, et al., Science **323**, 610 (2009).
- ³¹ N. P. Guisinger, G. M. Rutter, J. N. Crain, P. N. First, and J. A. Stroscio, Nano Lett. **9**, 1462 (2009).
- ³² D. K. Samarakoon and X. Q. Wang, ACS Nano **4**, 4126 (2010).
- ³³ A. I. Shkrebtii, E. Heritage, P. McNelles, J. L. Cabellos, and B. S. Mendoza, Phys. Stat. Sol. (c) **9**, 1378 (2012).
- ³⁴ M. Gmitra, D. Kochan, and J. Fabian, Phys. Rev. Lett. **110**, 246602 (2013).
- ³⁵ R. Zapata-Peña, S. M. Anderson, B. S. Mendoza, and A. I. Shkrebtii, physica status solidi (b) **253**, 226 (2016).
- ³⁶ S. F. Alvarado, H. Riechert, and N. E. Christensen, Phys. Rev. Lett. **55**, 2716 (1985).
- ³⁷ B. Schmiedeskamp, B. Vogt, and U. Heinzmann, Phys. Rev. Lett. **60**, 651 (1988).
- ³⁸ F. Nastos, B. Olejnik, K. Schwarz, and J. E. Sipe, Phys. Rev. B **72**, 045223 (2005).
- ³⁹ F. Nastos, J. Rioux, M. Strimas-Mackey, B. S. Mendoza, and J. E. Sipe, Phys. Rev. B **76**, 205113 (2007).
- ⁴⁰ X. Gonze, B. Amadon, P. M. Anglade, J. M. Beuken, F. Bottin, P. Boulanger, F. Bruneval, D. Caliste, R. Caracas, M. Côté, et al., Comput. Phys. Commun. **180**, 2582 (2009).
- ⁴¹ C. Hartwigsen, S. Goedecker, and J. Hutter, Phys. Rev. B **58**, 3641 (1998).

⁴² M. Wojtaszek, I. J. Vera-Marun, T. Maassen, and B. J. van Wees, Phys. Rev. B **87**, 081402 (2013).

⁴³ C. Ertler, S. Konschuh, M. Gmitra, and J. Fabian, Phys. Rev. B **80**, 041405 (2009).